JACS
JOURNAL OF THE AMERICAN CHEMICAL SOCIETY
pubs.acs.org/JACS
Article

Speciation of Cu Surfaces During the Electrochemical CO Reduction Reaction

Yaran Zhao,[†] Xiaoxia Chang,[†] Arnav S. Malkani, Xuan Yang, Levi Thompson,* Feng Jiao,* and Bingjun Xu*

Cite This: J. Am. Chem. Soc. 2020, 142, 9735−9743
Read Online
ACCESS | Metrics & More | Article Recommendations | Supporting Information

ABSTRACT: Cu-catalyzed selective electrocatalytic upgrading of carbon dioxide/monoxide to valuable multicarbon oxygenates and hydrocarbons is an attractive strategy for combating climate change. Despite recent research on Cu-based catalysts for the CO_2 and CO reduction reactions, surface speciation of the various types of Cu surfaces under reaction conditions remains a topic of discussion. Herein, in situ surface-enhanced Raman spectroscopy (SERS) is employed to investigate the speciation of four commonly used Cu surfaces, i.e., Cu foil, Cu micro/nanoparticles, electrochemically deposited Cu film, and oxide-derived Cu, at potentials relevant to the CO reduction reaction in an alkaline electrolyte. Multiple oxide and hydroxide species exist on all Cu surfaces at negative potentials, however, the speciation on the Cu foil is distinct from that on micro/nanostructured Cu. The surface speciation is demonstrated to correlate with the initial degree of oxidation of the Cu surface prior to the exposure to negative potentials. Combining reactivity and spectroscopic results on these four types of Cu surfaces, we conclude that the oxygen containing surface species identified by Raman spectroscopy are unlikely to be active in facilitating the formation of C_{2+} oxygenates in the CO reduction reaction.

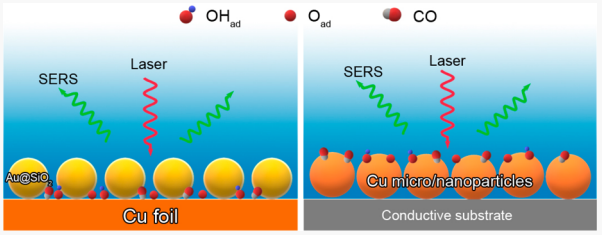

INTRODUCTION

Electrochemical CO_2 and CO reduction reactions (CO_2RR and CORR) are widely recognized and extensively investigated as a potential strategy to use anthropogenic CO_2 as an alternative carbon source to produce fuels and chemicals and thus reduce its emissions to the atmosphere.[1−4] Cu is the only metal capable of directly converting CO_2 and CO to valuable oxygenates and hydrocarbons with high selectivities, and therefore much effort has been devoted into understanding Cu-based catalysts.[5−9] However, key aspects of the fundamental understanding that could enable rapid future catalyst design and engineering remain unclear, among which two questions are at the center of recent discussion in the literature:[10−17] (1) speciation of Cu surfaces, e.g., surface oxides, hydroxides, and subsurface oxygen, at conditions relevant to the CO_2RR and the CORR; and (2) roles of these surface species in promoting these two reactions. The difficulty in addressing the first question largely lies in the challenge of characterizing the surface speciation at reaction conditions, i.e., in the presence of electrolytes and at reducing electrode potentials. Since bulk Cu oxide and hydroxide phases are known to be unstable at potentials relevant to the CO_2RR and the CORR,[18] oxygen-containing species are likely to be present only in the form of thin layers or patches of surface species, if at all. Thus, only in situ/operando techniques with high interfacial specificity are expected to yield reliable information. For example, any ex situ characterization involving ambient exposure of Cu surfaces, regardless of how fleeting, is unlikely to produce conclusive results, owing to the possibility of the surface oxidation by trace amounts of O_2. This is because the open circuit potential (OCP, ∼0.65 V vs RHE at pH = 11.7, all potentials in this work are referred to the reversible hydrogen electrode, or RHE, scale) is typically sufficiently high to oxidize Cu with trace amounts of O_2.

Moreover, no single in situ/operando technique is able to provide a complete picture of the interface, and thus results from multiple such characterizations are needed. For example, our recent work employed operando surface enhanced infrared spectroscopy (SEIRAS) to investigate the surface sites available with CO as the probe molecule,[19] and showed that oxide-derived Cu (OD-Cu) preferentially exposed Cu(100) like facets key to the C−C coupling chemistry in the CORR. Since surface metal−oxygen/carbon (M−O/M−C) vibrations are invisible to SEIRAS, if they exist at the CORR conditions, their impact on reactivity cannot be assessed using this technique. This specific point will be systematically investigated with in situ surface-enhanced Raman spectroscopy (SERS) in this

Received: February 28, 2020
Published: April 27, 2020

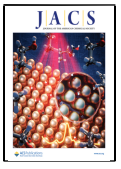

https://dx.doi.org/10.1021/jacs.0c02354
J. Am. Chem. Soc. 2020, 142, 9735−9743

work. An often overlooked fact in interpreting results from in situ/operando experiments is that they often involve special sample preparation procedures and spectral cell configurations, which could render the results less representative of the state of catalysts in the reactivity studies. A good example is that most SEIRAS spectroelectrochemical cells are unstirred, which could cause mass transport limitations and skew the spectral observations, as demonstrated in our recent work.[20] Another example is that the preparation of SEIRAS active Cu surfaces typically involves chemically depositing a thin Cu layer on a Si surface,[21−23] and whether this type of Cu surface is representative of the surface of Cu foils and particles commonly used in reactivity studies is implicitly assumed but remains unverified. Similar challenges exist for SERS when electrochemically roughened surfaces are prepared to generate surface enhancing features.[24] The advent of shell-isolated nanoparticles, e.g., silica encapsulated Au nanoparticles (Au@SiO_2),[25] as inert surface signals enhancing agents provides an effective strategy to conduct SERS investigations without the need to modify catalysts' surface morphologies. Despite the challenges discussed regarding the identification of surface species, understanding their roles in the reaction could be an even more daunting task. This requires comprehensive knowledge of the various species present at the reaction conditions, and establishes quantitative correlations between densities of various species and rates/selectivities. Meanwhile, it is less burdensome to show specific surface species to be spectators in the reaction of interest by demonstrating the lack of consistent reactivity trend with the absence/presence, absolute density, or relative surface coverage of the species.

In this work, we employ in situ SERS to investigate the speciation of five common Cu surfaces, i.e., Cu foil, Cu microparticles (Cu MPs), Cu nanoparticles (Cu NPs), chemically deposited Cu film on Si (Chem-Cu), and OD-Cu, and correlate the spectral observation with their CORR performance. Multiple Cu oxide and hydroxide species are identified on all of the Cu surfaces investigated at potential as negative as −0.8 V. The nature and relative abundance of surface species on Cu foil are distinct from micro/nano-structured Cu surfaces. The difference in the surface speciation of Cu is attributed to the initial oxidation state of the surface prior to the exposure to the reducing potential. Combined with the complementary CORR reactivity results, we conclude that the presence of the $CuO_x/(OH)_y$ phase is unlikely the origin of OD-Cu's unique ability to produce C_{2+} oxygenates.

RESULTS AND DISCUSSION

In situ Raman spectroscopy shows that Cu foils do not possess the surface enhancement effect, and shell-isolated nanoparticle-enhanced Raman spectroscopy (SHINERS) is necessary to detect surface species at different electrode potentials. Raman spectra on a Cu foil (Figures 1a and S1a of the Supporting Information, SI) show no feature in the cathodic potential steps from the OCP (~0.65 V) to −0.8 V in the CO atmosphere, except for a band at 980 cm^{-1} attributable to the sulfate ion in the bulk electrolyte.[26] The lack of spectral feature of surface species on the bare Cu foil could be explained by the following two possible reasons: (1) no Raman-active surface species is present at the Cu surface in the entire potential window investigated in this work; and (2) the Cu foil does not possess the capability of enhancing the Raman signal at the surface, or enabling SERS. The first possibility contradicts the common knowledge that Cu surfaces possess a native oxide

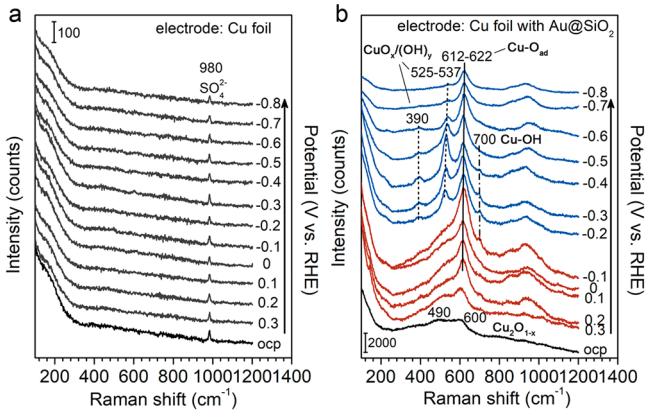

Figure 1. (a) In situ Raman spectra and (b) in situ SHINER spectra of a Cu foil at indicated potentials in CO saturated KOH/K_2SO_4 electrolyte (0.01 M KOH and 0.045 M K_2SO_4, pH = 11.7). The spectra were collected on a cathodic sequence of potential steps from OCP to −0.8 V in 0.1 V intervals.

layer upon exposure to ambient air, which has been confirmed in multiple works.[27−29] The relatively flat surface of Cu foil (Figure S2a) supports the second explanation because the SERS effect is typically generated on rough surfaces, especially at hot spots such as tips, edges, and gaps between two nanoparticles.[30−32] To test this hypothesis, Au@SiO_2 nanoparticles are introduced to the Cu foil surface to enable SHINERS (Figures 1b and S1b).[25] Au@SiO_2 particles are synthesized according to a reported method[33] (Figure S2b, inset), with an Au core (50 ± 5 nm in diameter) and a SiO_2 shell (2.0 ± 1.0 nm in thickness). Unless otherwise noted, the electrolyte used throughout the spectroscopic study is composed of 0.01 M KOH and 0.045 M K_2SO_4 (pH = 11.7), which ensures a reasonable ionic conductivity and minimizes the damage of the SiO_2 shell of Au@SiO_2 in the strongly alkaline conditions. No vibrational band attributable to CO adsorbed on Au (~2100 cm^{-1}) is observed in any experiment reported in this work, suggesting the absence of exposed Au surface on Au@SiO_2.[34] Indeed, in situ SHINERS on the Cu foil reveals multiple surface species present at various potentials (Figure 1b). At the OCP, two broad bands at ~490 and ~600 cm^{-1} attributable to the surface Cu oxide phase are present. These spectral features do not match any stoichiometric Cu oxide phases, i.e., CuO and Cu_2O,[16] but are similar to those of the partially reduced Cu_2O phase (see below). These bands persist to as low as −0.1 V and are assigned to Cu_2O_{1-x}. The presence of these bands shows that the utilization of Au@SiO_2 enables the selective detection of surface species.

SHINERS results of Cu foil at reducing potentials relevant to the CORR show that $Cu(OH)_x$ and CuO_x species persist at as low as −0.8 V. A peak centered at 612 cm^{-1} appears at 0.3 V on the Cu foil, which grows in intensity and blueshifts to 620 cm^{-1} as the potential decreases to −0.1 V (Figure 1b). Its intensity attenuates and the peak position shifts to 622 cm^{-1} as the potential further decreases to −0.8 V. This Raman band is assigned to a $Cu-O_{ad}$ stretching mode rather than a Cu−OH mode, because of the lack of shift when replacing H_2O with D_2O (Figure S3). This is also consistent with a recent study assigning the Raman bands at 570−630 cm^{-1} on Cu(111) to the $Cu-O_{ad}$ species.[26] The broad band located between 800 and 1000 cm^{-1} appears to vary concurrently with the band at 612−622 cm^{-1}, which likely originates from the same surface

https://dx.doi.org/10.1021/jacs.0c02354
J. Am. Chem. Soc. 2020, 142, 9735−9743

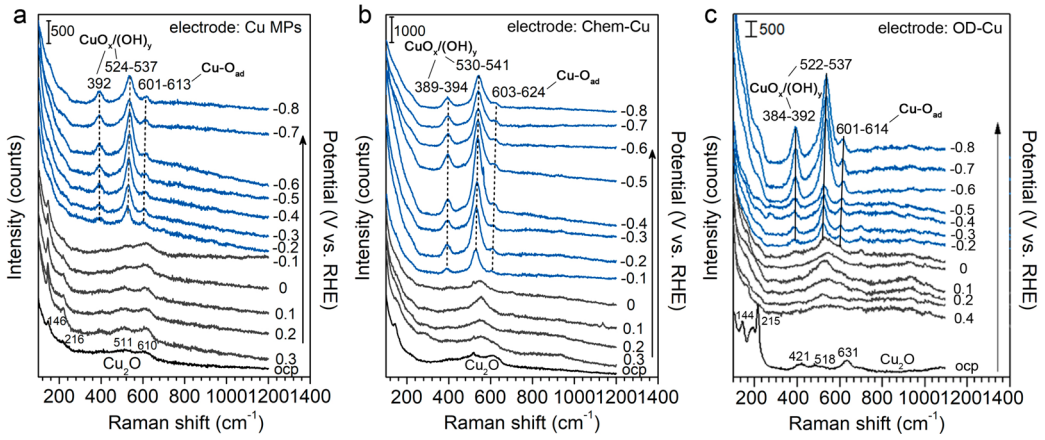

Figure 2. Potential-dependent Raman spectra of (a) Cu MPs, (b) Chem-Cu, and (c) OD-Cu in CO saturated KOH/K_2SO_4 electrolyte. The spectra were collected during a cathodic sequence of potential steps from the OCP to −0.8 V.

species. In addition, a new peak at 525 cm^{-1}, which has been previously assigned to a Cu−OH mode,[26,35] arises and the intensity reaches its maximum at −0.4 V. This band also blueshifts as the potential becoming more negative, and largely disappears at potentials <−0.6 V. This band only redshifts 7 cm^{-1} in D_2O as compared to in H_2O, which differs from a ∼30 cm^{-1} redshift observed for a band at a similar location in a previous report.[26] Therefore, we tentatively attribute this band to the mixed Cu oxide and hydroxide species as $CuO_x/(OH)_y$, which will be discussed further later in this work. The band centered at 390 cm^{-1} appears at the same potential as the band at 525 cm^{-1}, and the intensities of the two bands vary in sync, indicating a shared origin. A weak band centered at 700 cm^{-1} that appears between −0.1 V and −0.4 V has also been assigned to surface hydroxyl species, referred to as Cu-$(OH)_x$.[26,36,37] A band attributable to linearly bonded CO appears in the range of 2053−2070 cm^{-1} between 0.1 and −0.2 V (Figure S1b). Another band at 1863−1873 cm^{-1} corresponding to bridge-bonded CO appears at more negative potentials accompanied by the disappearance of the linearly bonded CO (Figure S1b). These observations are largely in line with previous Raman studies on Cu.[15,22] It is worth noting that the adsorbed CO band only appears after the Cu_2O_{1-x} phase is reduced, suggesting that CO adsorption is not feasible on partially reduced oxide species layer of the Cu surface. We note that only peaks associated with metallic Cu are observed in the XRD pattern of the Cu foil (Figure S4), indicating the lack of long-range ordered crystalline phases of oxide or hydroxide on the surface.

While the main spectral features of the Cu foil are generally consistent, there are considerable variations in the relative intensities of spectral features depending on the locations at which spectra are collected. Raman spectra in this work are acquired with a confocal microscope with a focal spot of ∼2 μm in diameter, which is common in similar studies.[25,38] Thus, the spectra collected only reflect the state of the part of the surface sampled. To probe the spatial variation of the Cu foil at the same potential, 10 spots are sampled at each potential on the Cu foil (Figure S5). Although the general features in the spectra are similar, the relative intensities of individual bands do vary, which is likely caused by the inhomogeneity of the surface rather than the distribution of Au@SiO_2 particles. The distribution of Au@SiO_2 particles on the Cu foil is generally uniform (Figure S2b), and the minor aggregation of Au@SiO_2 particles should only impact the intensity, rather than the line shape of the observed Raman features. The average distance between Au@SiO_2 particles is much smaller than 2 μm, which indicates that the SERS signal obtained will be an average enhancing effect induced by the majority of isolated and minority of aggregated Au@SiO_2 particles. A similar level of spectral variations is observed on micro/nanostructured Cu samples that do not require Au@SiO_2 particles for SERS, confirming that the spectral variation is due to the surface inhomogeneity. These spatial variations in Raman spectra on Cu surfaces could at least in part explain different spectral features reported in the literature.[26] Therefore, it is important to collect SERS spectra at multiple locations to ensure the spectral features are not caused by anomalies at the specific area of the surface. Raman spectra are collected at multiple locations (≥3) on all samples and at all potentials investigated in this work. We note that the pretreatment with HCl[39,40] makes spectra collected on the Cu foil surface more uniform than those on the sample without the treatment at any given potential (Figure S6). The absence of Cu−Cl vibrational band (270−290 cm^{-1})[37,41] in Figure 1 and the control experiment with Cl^- containing electrolyte both indicate that the presence of Cl^- in HCl in the pretreatment does not impact the spectral feature.

The presence of CO impacts the surface speciation on the Cu foil at reducing potentials. Only a band at 709 cm^{-1} attributable to $Cu(OH)_x$ is observed on the Cu foil (with Au@SiO_2) at potentials between 0.1 V to −0.4 V in Ar saturated electrolyte (Figure S7), which is consistent with a recent report.[26] The clear difference in the spectra at reducing potentials on the Cu foil in CO and Ar is in sharp contrast to the similar cyclic voltammograms on Cu in both atmospheres (Figure S8). This indicates that cyclic voltammetry is not sufficiently sensitive to differentiate subtle changes in the speciation of the Cu foil surface caused by the presence of CO. Adsorbed CO appears to induce the formation of and/or stabilize the surface $Cu(OH)_x$ and CuO_x phases on the Cu foil at reducing potentials.

In addition to Cu foil, in situ Raman spectroscopy is also employed to probe the surface speciation of micro/nanostructured Cu catalysts frequently used in the CO_2RR and the CORR research, i.e., Cu MPs (0.1−2 μm), Cu NPs (25−100 nm), Chem-Cu on Si, and OD-Cu. Cu MPs and NPs are purchased and used without further treatment, as in several

https://dx.doi.org/10.1021/jacs.0c02354
J. Am. Chem. Soc. 2020, 142, 9735−9743

recent studies.[42,43] These different types of Cu surfaces are commonly used in the CO_2RR and the CORR in both batch and flow cell configurations due to their ease of integration with gas diffusion layers.[43,44] Chem-Cu is chemically deposited on the Si surface, which is frequently used in SEIRAS investigations of the CO_2RR and the CORR.[19−22] OD-Cu is known for its ability to produce multicarbon products at lower overpotential than untreated Cu surfaces.[44,45] Here, OD-Cu is prepared by electrochemically reducing a Cu_2O layer on a Cu substrate. Detailed preparation procedures and representative morphologies of samples are provided in the SI (Figure S9). As expected, Cu foil, MPs, NPs, Chem-Cu, and OD-Cu all exhibit characteristic XRD patterns of polycrystalline Cu (Figure S4). Peaks corresponding to Cu_2O appear on the XRD pattern of Cu NPs, which is likely due to the propensity of nanoparticles for oxidation when exposed to air. The cyclic voltammograms (CVs) of these Cu surfaces show similar general redox features (Figures S8 and S10), which are consistent with literature reports.[37,46]

Although micro/nanostructured Cu, as well as Cu foil, are generally believed to exhibit similar polycrystalline Cu surfaces, Raman spectra of micro/nanostructured Cu at negative potentials show distinct features from those of the Cu foil. Cu MPs, NPs, Chem-Cu, and OD-Cu all exhibit a surface enhancement effect for Raman spectroscopy, and Au@SiO_2 is not necessary to observe Raman features of surface species (Figures 2, S11, and S12), as suggested in several recent works.[15,17,47,48] This is expected as the particulate morphology has been shown to be SERS active.[49] Control experiments show that the Raman spectra on these samples with and without Au@SiO_2 are identical within the experimental errors (Figures 2a and S13). Thus, it is reasonable to conclude that Raman spectra of Cu MPs, NPs, Chem-Cu, and OD-Cu without Au@SiO_2 do not selectively enhance the Raman signal of a subset of surface species because all Raman active surface species should be probed with Au@SiO_2 in SHINERS. At the OCP, multiple peaks attributable to surface Cu_2O at 146, 216, 415, 511, and 610 cm^{-1} are present on the surface of Cu MPs (Figure 2a), which agree with the bands observed on the electrodeposited Cu_2O film, the precursor of OD-Cu (Figure 2c), and are also consistent with the literature.[26] Compared to the Cu_2O_{1-x} species present on the Cu foil at the OCP (Figure 1b), the bands attributable to surface Cu_2O are more well-defined on Cu MPs, suggesting a higher degree of surface oxidation (Figure 2a). This is not surprising because the density of undercoordinated surface atoms, which are more susceptible to oxidation upon air exposure, increases as the particle size decreases. The appearance of XRD peaks corresponding to Cu_2O on Cu NPs, which are absent in other forms of Cu surfaces investigated (Figure S4), supports this line of reasoning. The surface Cu_2O phase on Cu MPs persists until −0.1 V in the CO atmosphere, and all corresponding Raman features disappear at −0.2 V or below, indicating its full reduction. This is consistent with Soriaga's work which shows reduction of native oxide at −0.9 V vs standard hydrogen electrode in KOH (∼−0.2 V vs RHE).[50] Cu MPs and foil show distinct Raman features at potentials below −0.2 V, suggesting differences in the distribution of surface species. At −0.2 V, three well-defined bands appear simultaneously at 392, 524, and 601 cm^{-1} on Cu MPs. Importantly, the relative intensity of 524 and 601 cm^{-1} bands on the Cu MPs is the opposite of that on the Cu foil, with the former as the dominant feature. When conducting in D_2O instead of H_2O, the peaks at 392 and 530 cm^{-1} under −0.4 V exhibit redshifts to 385 and 523 cm^{-1}, respectively (Figure S14), indicating that both bands correspond to normal modes involving at least one proton. The smaller redshift (7 cm^{-1}) than that reported previously (30 cm^{-1}) for Cu hydroxide species indicates that there might be surface adsorbed oxygen, which plays a constructive role in bending the H atoms, near the hydroxyl group.[32,51] Such a coadsorbed species is likely a mixed Cu oxide and hydroxide species, i.e., $CuO_x/(OH)_y$, similar to those observed on the Cu foil. A similar assignment of these bands at 527/523 cm^{-1} to a patina-like mixed phase containing oxides and/or hydroxide and/or carbonate has been suggested in the literature.[27] Meanwhile, the band at 601 cm^{-1} displays a negligible shift in D_2O, which confirms its assignment of $Cu-O_{ad}$ species as that on Cu foil (Figure 1b).[16] All peaks assignments and the comparison with reported literatures are summarized in Table S1. Only bridge-bonded CO at 1857−1870 cm^{-1} is detected at potentials below −0.1 V (Figure S11a). Similar to the case of Cu foil, it can be inferred that at potentials >−0.2 V, the presence of oxide phases on Cu MPs prevents the adsorption of CO. This is supported by the observation that adsorbed CO persists up to 0.2 V in the anodic potential step due to the lack of the native oxide (Figure S15). On the basis of the relative intensities of the Raman bands in the same spectra, $CuO_x/(OH)_y$ is more abundant on Cu MPs than foil at potentials below −0.1 V, while the opposite is true for $Cu-O_{ad}$. We note that the relative intensities of Raman bands cannot be used to infer absolute coverages of surface species due to the unknown scattering cross sections for different modes, i.e., the coverage of $CuO_x/(OH)_y$ could be lower than that of $Cu-O_{ad}$ even though its Raman band is more intense or vice versa. In contrast to the results on the Cu foil, Raman spectra on Cu MPs at reducing potentials in CO and Ar saturated electrolytes are similar (Figures 2a and S16), suggesting that the presence of CO does not impact the surface speciation on Cu MPs. Spectral features of Chem-Cu and Cu NPs (Figures 2b and S12) in the potential range of OCP to −0.8 V are similar to those of Cu MPs, suggesting the presence of similar surface species. This suggests that micro/nanostructured Cu share similar surface species at potentials relevant to the CORR. Upon reduction, the Raman spectra of the electrodeposited Cu_2O layer, i.e., OD-Cu, also resemble those from other micro/nanostructured Cu materials (Figure 2c). A common feature of micro/nanostructured Cu is that there is a relatively well-defined surface Cu_2O layer at the OCP, while the oxide layer of the Cu foil at the OCP is composed of a more reduced oxide phase (Cu_2O_{1-x}). Thus, we hypothesize that the initial state of the Cu catalyst has a substantial impact on the surface speciation at reducing potentials.

To investigate the impact of the surface oxidation state of Cu catalysts prior to the exposure to reducing potentials on its speciation at negative potentials, in situ Raman spectra are collected with a square wave potential profile. During this process, a Cu foil is exposed to increasingly positive potentials for 5 min and followed by a cathodic step to −0.4 V for 5 min (redox currents typically reach a stable value within 5 min, Figure 3a). Raman spectra are collected at the end of each positive potential segment and −0.4 V (Figure 3b and c). No Au@SiO_2 is introduced to the Cu foil in this experiment, and the appearance of Raman features reflects the development of nanostructures that enable the surface enhancement effect in the redox treatment. Consistent with the results in Figure 1, no

https://dx.doi.org/10.1021/jacs.0c02354
J. Am. Chem. Soc. 2020, 142, 9735−9743

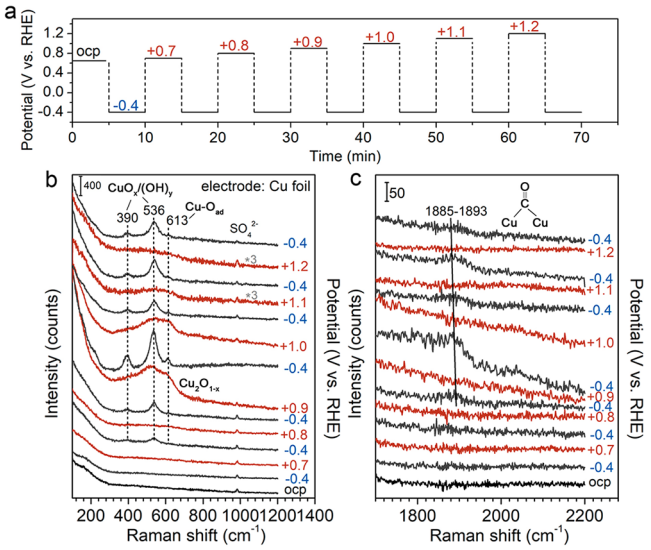

Figure 3. (a) Square wave potential profile applied on Cu foil electrode in CO saturated KOH/K_2SO_4 electrolyte. (b) In situ Raman spectra of Cu foil collected after 5 min holding at each oxidative/reduced potential presented in a. (c) Corresponding Raman spectra of CO adsorption on Cu foil at each potential shown in a.

discernible Raman signal of surface species is observed during the potential hold at the OCP and the subsequent hold at −0.4 V presumably due to the lack of SERS activity of the flat surface of the newly polished and HCl treated Cu foil. Similarly, no Raman signal is present at the end of the 5 min hold under 0.7 V, but weak bands corresponding to $CuO_x/(OH)_y$ appear at the ensuing potential hold at −0.4 V. This is likely due to the roughening of the Cu surface in the redox cycle, which leads to the formation of SERS active microstructures.[52] We note that the morphology of Cu foil treated at up to 1.2 V observed by SEM does not exhibit discernible difference compared to the untreated one (Figure S17), suggesting that the surface enhancing structure is either nanometer-scale in dimension (beyond the spatial resolution of SEM) or the features generated at negative potentials are destroyed by upon air exposure prior to the SEM measurements. The most intense Raman feature of the Cu foil after exposure to oxidizing potentials (>0.7 V) corresponds to $CuO_x/(OH)_y$, rather than CuO_x (Figure 1b). This is a clear indication that the exposure to oxidizing potentials, or the redox history of the catalyst, could impact the nature and distribution of surface species present at reducing conditions. Weak and broad bands corresponding to Cu_2O_{1-x} are present at the end of the subsequent potential hold at 0.8 V, which is likely caused by the increase in the coverage of Cu_2O_{1-x} after the potential hold and the enhanced SERS effect with the roughened surface. This trend is more obvious after the potential hold at 0.9 V, in which strong bands corresponding to the Cu_2O_{1-x} phase are present, and intense bands at 390, 536, and 613 cm^{-1} are observed after the subsequent potential hold at −0.4 V. These bands are similar to those observed on Cu MPs, NPs, Chem-Cu, and OD-Cu at the same potential, supporting the hypothesis that the key difference between the surface speciation at reducing potentials on Cu foil and micro/nanostructured Cu is the surface oxidation state prior to the reduction. Only the bridge-bonded CO band (1885−1893 cm^{-1}) is detected after the Cu foil is exposed to potentials above 0.7 V, which is likely due to the enhancement of the SERS effect upon the exposure to higher potential. Further increasing the oxidizing potential above 0.9 V, the intensity of the Cu_2O_{1-x} phase bands at positive potential and also the $CuO_x/(OH)_y$ species at −0.4 V are largely leveled off. Regardless, the spectral features at −0.4 V in all cases resemble those of micro/nanostructured Cu. Since electrochemical redox cycling leads to higher CO_2RR and CORR reactivity and selectivity to C_{2+} products,[53] the changed surface species at reducing potentials, e.g., OH bound to Cu surface, has been proposed to benefit the reduction of CO_2 and the production of C_{2+} products.[48] A similar experiment with the same potential profile on Cu MPs shows little change in the Raman spectra collected at the end of the potential hold at high and low potentials, suggesting that the redox cycling does not modify the surface speciation of Cu MPs (Figure S18). This is likely due to the surface of Cu MPs upon air exposure is sufficiently oxidized to induce the formation of the $CuO_x/(OH)_y$ species at reducing potentials. The dominant surface species on each catalyst observed from in situ Raman are concluded in Table 1.

In order to correlate the species present on Cu catalysts at reducing potentials with the CORR performance, the CORR performance of all Cu surfaces investigated is evaluated in a batch cell. Cu foil, MPs, NPs, Chem-Cu and OD-Cu are employed as working electrodes in CO saturated 0.1 M KOH at −0.6 V to highlight the impact of catalysts on the yields of C_{2+} products. Cu foil shows the worst CORR performance with the highest Faradaic efficiency (FE) for the side product H_2 (84.6%), and the lowest FE for ethylene (0.68%, brown bars in Figure 4). More ethylene is produced on the surface of Cu MPs (2.03%, gray) and Chem-Cu (3.78%, green) than on the bare Cu foil, however, without any detectable amount of liquid product. OD-Cu, in contrast, could produce more ethylene (5.64%) as well as the liquid products of ethanol and n-propanol with the FEs of 4.34% and 0.41%, respectively (blue bars in Figure 4), which is consistent with the literature and suggests the reduction of overpotential needed for multicarbon products.[54−56] Cu NPs' product distribution is close to the average of that of Cu MPs and OD-Cu, which is not surprising as Cu NPs are more deeply oxidized than Cu MPs but less so than Cu_2O (precursor to OD-Cu) before exposing to the reducing condition in the CORR. Cu MPs, NPs, and OD-Cu evaluated in the flow-cell configuration, in which the gaseous reactant is directly fed to the electrode−electrolyte interface to form a triple-phase boundary, also show distinct product distributions (Figure S19), especially at low overpotentials (≥−0.6 V vs RHE). At −0.6 V, the combined

Table 1. Major Surface Species on Cu at Indicated Potentials Identified by Raman Spectroscopy

Cu catalysts	OCP	−0.4 V (vs RHE)
Cu foil	Cu_2O_{1-x}	CuO_x
Cu foil after oxidized at +0.9 V	Cu_2O_{1-x}	$CuO_x/(OH)_y$
Cu micro/nanoparticles Chem-Cu OD-Cu	Cu_2O	$CuO_x/(OH)_y$

https://dx.doi.org/10.1021/jacs.0c02354
J. Am. Chem. Soc. 2020, 142, 9735−9743

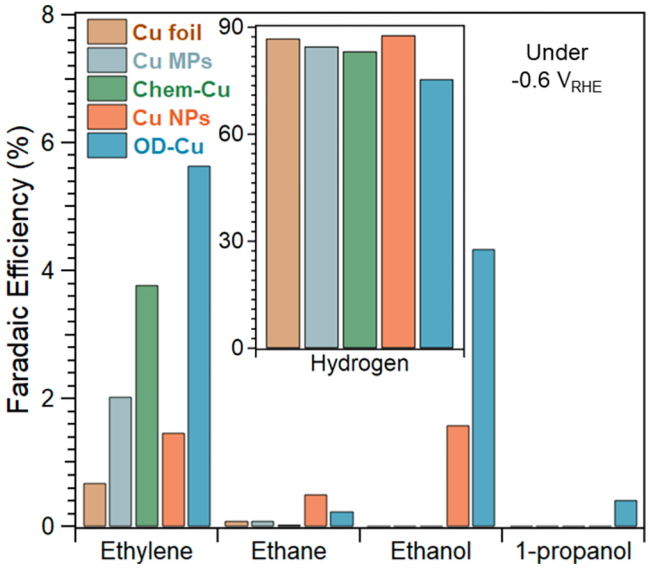

Figure 4. Comparison of product Faradaic efficiency between CORR on Cu foil (brown), Cu MPs (gray), Chem-Cu (green), Cu NPs (orange), and OD-Cu (blue) in CO sat. 0.1 M KOH under −0.6 V.

FE for C_{2+} products on these three catalysts parallels that of batch results: OD-Cu > Cu NPs > Cu MPs. All samples tested in the flow cell show much higher FEs to the CORR products than in the batch cell, which is expected with the improved mass transport of CO to the triple-phase boundary. We note that the OD-Cu used in the flow cell experiments is prepared by a different procedure due to the need to deposit on the Cu support, but previous reports have shown they show similar reactivities.[44,54]

It is noteworthy that although Cu MPs, NPs, Chem-Cu and OD-Cu have similar Raman features for $CuO_x/(OH)_y$ species under −0.6 V (Figures 2 and S12), OD-Cu is unique in its ability to produce C_{2+} oxygenates at this potential (Figure 4, blue). This is a strong indication that the surface $CuO_x/(OH)_y$ species is not active in facilitating the formation of multicarbon oxygenates in the CORR. Meanwhile, all micro/nanostructured Cu samples exhibit a higher FE for ethylene than that on Cu foil, suggesting a potential promotional role of this phase in the ethylene formation. Following the same logic, the surface CuO_x species on Cu foil (Figure 1b) is also unlikely to be active in the CORR. Since SERS is not a quantitative technique, by itself it is insufficient to establish a quantitative correlation between the density or surface coverage of a species with the production rate of one or a group of products expected of rigorous structure−activity relations. However, the criterion for the proof against a species as the active phase for a reaction is demanding, i.e., inconsistency between experimental results and any key predictions based on the assumption of this species being the active phase would suffice. The relative intensities between bands corresponding to $CuO_x/(OH)_y$ and CuO_x species on all micro/nanostructured Cu catalysts in the same spectra at potentials relevant to the CORR are similar (Figure 2), suggesting the relative abundances of these two species across all micro/nanostructured Cu surfaces under reaction conditions are comparable. While SERS results do not allow for the determination of absolute densities of these surface species, it is clear that variations in the site density alone cannot account for the different product distributions observed in both batch and flow reactors (Figures 4 and S19).

In addition, despite the marked difference in the relative abundance of $CuO_x/(OH)_y$ and CuO_x species (Figures 1b and 2a), both Cu foil and Cu MPs produce ethylene as the only C−C coupling product. The slightly higher FE for ethylene on Cu MPs than that of Cu foil could be reasonably attributed to its higher surface area. Thus, the relative abundance of these two observed oxygen-containing surface Cu species does not appear to impact the production of oxygenated C−C coupling products.

The combination of the spectroscopic and reactivity results suggest that oxygen-containing species do exist on Cu catalysts at potentials relevant to the CORR, but do not appear to play any major role in facilitating C−C coupling pathways. It follows that the composition of these species is not diagnostic of other structure changes induced by the redox retreatment at varying conditions that directly impact the CORR performance. It is worth noting that these conclusions drawn from in situ SERS, as for any other techniques, investigations are limited by the detection limit of this technique. It is known that trace amounts of additives or contaminants could drastically change the rate and product distribution of catalysts,[57,58] and the possibility of trace oxygen containing Cu species that exist below the detection limit of SERS playing a decisive role in the CORR, though remote, cannot be ruled out completely. In addition, although no appreciable change in the spectral feature at −0.6 to −0.8 V is observed, the typical time scale of the spectroscopic experiments (~1 h) does not allow for claims regarding the long-term stability of oxygen-containing Cu species at the reducing conditions. Our recent SEIRAS work showed that the CO adsorption sites are markedly different on Cu MPs and OD-Cu surfaces.[19] Combining the Raman results in this work and previous SEIRAS observations,[19] the preferential exposure favorable metallic facets, e.g., Cu(100), is likely responsible for OD-Cu's unique CORR activity.

CONCLUSIONS

In summary, in situ SERS investigations show that surface oxygen-containing species indeed exist in the alkaline electrolyte at potentials relevant to the CORR on all types of Cu surfaces investigated in this work. However, the relative abundance of surface CuO_x on Cu foils is higher than that on micro/nanostructured Cu, while the opposite is true for the surface $CuO_x/(OH)_y$ species. The presence of CO is necessary to stabilize surface oxide/hydroxide species on the Cu foil but not for micro/nanostructured Cu. The difference in the surface speciation on different types of Cu surfaces is demonstrated to be correlated to the initial degree of oxidation of the Cu surface prior to reduction. Combined with the reactivity results, we conclude that while CuO_x and $CuO_x/(OH)_y$ species do exist under the CORR conditions, but they are unlikely to be the active sites facilitating the formation of C_2 oxygenates.

ASSOCIATED CONTENT

Supporting Information

The Supporting Information is available free of charge at https://pubs.acs.org/doi/10.1021/jacs.0c02354.

Experimental details and supporting data (PDF)

https://dx.doi.org/10.1021/jacs.0c02354
J. Am. Chem. Soc. 2020, 142, 9735−9743

AUTHOR INFORMATION

Corresponding Authors

Levi Thompson − *Center for Catalytic Science and Technology, Department of Chemical & Biomolecular Engineering, University of Delaware, Newark, Delaware 19716, United States*; Email: ltt@udel.edu

Feng Jiao − *Center for Catalytic Science and Technology, Department of Chemical & Biomolecular Engineering, University of Delaware, Newark, Delaware 19716, United States*; orcid.org/0000-0002-3335-3203; Email: jiao@udel.edu

Bingjun Xu − *Center for Catalytic Science and Technology, Department of Chemical & Biomolecular Engineering, University of Delaware, Newark, Delaware 19716, United States*; orcid.org/0000-0002-2303-257X; Email: bxu@udel.edu

Authors

Yaran Zhao − *Center for Catalytic Science and Technology, Department of Chemical & Biomolecular Engineering, University of Delaware, Newark, Delaware 19716, United States*

Xiaoxia Chang − *Center for Catalytic Science and Technology, Department of Chemical & Biomolecular Engineering, University of Delaware, Newark, Delaware 19716, United States*; orcid.org/0000-0001-6598-6083

Arnav S. Malkani − *Center for Catalytic Science and Technology, Department of Chemical & Biomolecular Engineering, University of Delaware, Newark, Delaware 19716, United States*

Xuan Yang − *Center for Catalytic Science and Technology, Department of Chemical & Biomolecular Engineering, University of Delaware, Newark, Delaware 19716, United States*; orcid.org/0000-0001-8750-0742

Complete contact information is available at: https://pubs.acs.org/10.1021/jacs.0c02354

Author Contributions

†These authors contributed equally to this work.

Notes

The authors declare no competing financial interest.

ACKNOWLEDGMENTS

Y.Z. and L.T. acknowledge the support of the University of Delaware startup fund. X.C., A.M., and B.X. acknowledge the support of the National Science Foundation CAREER Program (Award No. CBET-1651625). F.J. thanks the National Science Foundation for financial support (Award No. CBET-1904966). The authors also thank Matthew Jouny for help with the reactivity tests in the flow cell. Authors thank GaossUnion (Tianjin) Photoelectric Technology Company for sharing the design of the in situ Raman cell.

REFERENCES

(1) IPCC. *Climate Change 2014: Synthesis Report. Contribution of Working Groups I, II and III to the Fifth Assessment Report of the Intergovernmental Panel on Climate Change*. Pachauri, R. K.; Meyer, L. A., Eds. IPCC: Geneva, Switzerland, 2014, 151 pp.

(2) Jouny, M.; Luc, W.; Jiao, F. General Techno-Economic Analysis of CO_2 Electrolysis Systems. *Ind. Eng. Chem. Res.* **2018**, *57*, 2165−2177.

(3) Gao, D.; Arán-Ais, R. M.; Jeon, H. S.; Roldan Cuenya, B. Rational catalyst and electrolyte design for CO_2 electroreduction towards multicarbon products. *Nat. Catal.* **2019**, *2*, 198−210.

(4) Zhang, H.; Chang, X.; Chen, J. G.; Goddard, W. A., III; Xu, B.; Cheng, M. J.; Lu, Q. Computational and experimental demonstrations of one-pot tandem catalysis for electrochemical carbon dioxide reduction to methane. *Nat. Commun.* **2019**, *10*, 3340.

(5) Luc, W.; Fu, X.; Shi, J.; Lv, J.-J.; Jouny, M.; Ko, B. H.; Xu, Y.; Tu, Q.; Hu, X.; Wu, J.; Yue, Q.; Liu, Y.; Jiao, F.; Kang, Y. Two-dimensional copper nanosheets for electrochemical reduction of carbon monoxide to acetate. *Nat. Catal.* **2019**, *2*, 423−430.

(6) Feng, X.; Jiang, K.; Fan, S.; Kanan, M. W. A Direct Grain-Boundary-Activity Correlation for CO Electroreduction on Cu Nanoparticles. *ACS Cent. Sci.* **2016**, *2*, 169−74.

(7) Kuhl, K. P.; Cave, E. R.; Abram, D. N.; Jaramillo, T. F. New insights into the electrochemical reduction of carbon dioxide on metallic copper surfaces. *Energy Environ. Sci.* **2012**, *5*, 7050−7059.

(8) Hori, Y.; Murata, A.; Takahashi, R. Formation of hydrocarbons in the electrochemical reduction of carbon dioxide at a copper electrode in aqueous solution. *J. Chem. Soc., Faraday Trans. 1* **1989**, *85*, 2309−2326.

(9) Dinh, C.-T.; Burdyny, T.; Kibria, M. G.; Seifitokaldani, A.; Gabardo, C. M.; De Arquer, F. P. G.; Kiani, A.; Edwards, J. P.; De Luna, P.; Bushuyev, O. S.; et al. CO_2 electroreduction to ethylene via hydroxide-mediated copper catalysis at an abrupt interface. *Science* **2018**, *360*, 783−787.

(10) Zhang, Y.; Guo, S.-X.; Zhang, X.; Bond, A. M.; Zhang, J. Mechanistic understanding of the electrocatalytic CO_2 reduction reaction − New developments based on advanced instrumental techniques. *Nano Today* **2020**, *31*, 100835.

(11) Luo, M.; Wang, Z.; Li, Y. C.; Li, J.; Li, F.; Lum, Y.; Nam, D.-H.; Chen, B.; Wicks, J.; Xu, A.; et al. Hydroxide promotes carbon dioxide electroreduction to ethanol on copper via tuning of adsorbed hydrogen. *Nat. Commun.* **2019**, *10*, 5814.

(12) Li, J.; Wu, D.; Malkani, A. S.; Chang, X.; Cheng, M.-J.; Xu, B.; Lu, Q. Hydroxide is not a Promoter of C_{2+} Product Formation in the Electrochemical Reduction of CO on Copper. *Angew. Chem., Int. Ed.* **2020**, *59*, 4464−4469.

(13) Schouten, K.; Kwon, Y.; Van der Ham, C.; Qin, Z.; Koper, M. A new mechanism for the selectivity to C_1 and C_2 species in the electrochemical reduction of carbon dioxide on copper electrodes. *Chem. Sci.* **2011**, *2*, 1902−1909.

(14) Tiwari, A.; Heenen, H. H.; Bjørnlund, A. S.; Maagaard, T.; Cho, E.; Chorkendorff, I.; Kristoffersen, H. H.; Chan, K.; Horch, S. Fingerprint Voltammograms of Copper Single Crystals under Alkaline Conditions: A Fundamental Mechanistic Analysis. *J. Phys. Chem. Lett.* **2020**, *11*, 1450−1455.

(15) Jiang, S.; Klingan, K.; Pasquini, C.; Dau, H. New aspects of operando Raman spectroscopy applied to electrochemical CO_2 reduction on Cu foams. *J. Chem. Phys.* **2019**, *150*, 041718.

(16) Deng, Y.; Handoko, A. D.; Du, Y.; Xi, S.; Yeo, B. S. In Situ Raman Spectroscopy of Copper and Copper Oxide Surfaces during Electrochemical Oxygen Evolution Reaction: Identification of Cu^{III} Oxides as Catalytically Active Species. *ACS Catal.* **2016**, *6*, 2473−2481.

(17) Chen, X.; Henckel, D. A.; Nwabara, U. O.; Li, Y.; Frenkel, A. I.; Fister, T. T.; Kenis, P. J. A.; Gewirth, A. A. Controlling Speciation during CO_2 Reduction on Cu-Alloy Electrodes. *ACS Catal.* **2020**, *10*, 672−682.

(18) Paracchino, A.; Laporte, V.; Sivula, K.; Grätzel, M.; Thimsen, E. Highly active oxide photocathode for photoelectrochemical water reduction. *Nat. Mater.* **2011**, *10*, 456−461.

(19) Malkani, A. S.; Dunwell, M.; Xu, B. Operando Spectroscopic Investigations of Copper and Oxide-Derived Copper Catalysts for Electrochemical CO Reduction. *ACS Catal.* **2019**, *9*, 474−478.

(20) Malkani, A. S.; Li, J.; Anibal, J.; Lu, Q.; Xu, B. Impact of Forced Convection on Spectroscopic Observations of the Electrochemical CO Reduction Reaction. *ACS Catal.* **2020**, *10*, 941−946.

(21) Gunathunge, C. M.; Ovalle, V. J.; Li, Y.; Janik, M. J.; Waegele, M. M. Existence of an Electrochemically Inert CO Population on Cu Electrodes in Alkaline pH. *ACS Catal.* **2018**, *8*, 7507−7516.
(22) Gunathunge, C. M.; Li, X.; Li, J.; Hicks, R. P.; Ovalle, V. J.; Waegele, M. M. Spectroscopic Observation of Reversible Surface Reconstruction of Copper Electrodes under CO_2 Reduction. *J. Phys. Chem. C* **2017**, *121*, 12337−12344.
(23) Heyes, J.; Dunwell, M.; Xu, B. CO_2 Reduction on Cu at Low Overpotentials with Surface-Enhanced in Situ Spectroscopy. *J. Phys. Chem. C* **2016**, *120*, 17334−17341.
(24) Tian, Z.-Q.; Ren, B.; Wu, D.-Y. Surface-Enhanced Raman Scattering: From Noble to Transition Metals and from Rough Surfaces to Ordered Nanostructures. *J. Phys. Chem. B* **2002**, *106*, 9463−9483.
(25) Li, J. F.; Huang, Y. F.; Ding, Y.; Yang, Z. L.; Li, S. B.; Zhou, X. S.; Fan, F. R.; Zhang, W.; Zhou, Z. Y.; Wu, D. Y.; Ren, B.; Wang, Z. L.; Tian, Z. Q. Shell-isolated nanoparticle-enhanced Raman spectroscopy. *Nature* **2010**, *464*, 392−395.
(26) Bodappa, N.; Su, M.; Zhao, Y.; Le, J. B.; Yang, W. M.; Radjenovic, P.; Dong, J. C.; Cheng, J.; Tian, Z. Q.; Li, J. F. Early Stages of Electrochemical Oxidation of Cu(111) and Polycrystalline Cu Surfaces Revealed by in Situ Raman Spectroscopy. *J. Am. Chem. Soc.* **2019**, *141*, 12192−12196.
(27) Smith, B.; Irish, D.; Kedzierzawski, P.; Augustynski, J. A Surface Enhanced Raman Scattering Study of the Intermediate and Poisoning Species Formed during the Electrochemical Reduction of CO_2 on Copper. *J. Electrochem. Soc.* **1997**, *144*, 4288−4296.
(28) Iijima, J.; Lim, J. W.; Hong, S. H.; Suzuki, S.; Mimura, K.; Isshiki, M. Native oxidation of ultra high purity Cu bulk and thin films. *Appl. Surf. Sci.* **2006**, *253*, 2825−2829.
(29) Lum, Y.; Ager, J. W. Stability of residual oxides in oxide-derived copper catalysts for electrochemical CO_2 reduction investigated with ^{18}O labeling. *Angew. Chem., Int. Ed.* **2018**, *57*, 551−554.
(30) Stiles, P. L.; Dieringer, J. A.; Shah, N. C.; Van Duyne, R. P. Surface-Enhanced Raman Spectroscopy. *Annu. Rev. Anal. Chem.* **2008**, *1*, 601−626.
(31) Xie, W.; Schlücker, S. Surface-enhanced Raman spectroscopic detection of molecular chemo- and plasmo-catalysis on noble metal nanoparticles. *Chem. Commun.* **2018**, *54*, 2326−2336.
(32) Dong, J.-C.; Zhang, X.-G.; Briega-Martos, V.; Jin, X.; Yang, J.; Chen, S.; Yang, Z.-L.; Wu, D.-Y.; Feliu, J. M.; Williams, C. T.; Tian, Z.-Q.; Li, J.-F. In situ Raman spectroscopic evidence for oxygen reduction reaction intermediates at platinum single-crystal surfaces. *Nat. Energy* **2019**, *4*, 60−67.
(33) Li, J. F.; Tian, X. D.; Li, S. B.; Anema, J. R.; Yang, Z. L.; Ding, Y.; Wu, Y. F.; Zeng, Y. M.; Chen, Q. Z.; Ren, B.; Wang, Z. L.; Tian, Z. Q. Surface analysis using shell-isolated nanoparticle-enhanced Raman spectroscopy. *Nat. Protoc.* **2013**, *8*, 52−65.
(34) Dunwell, M.; Lu, Q.; Heyes, J. M.; Rosen, J.; Chen, J. G.; Yan, Y.; Jiao, F.; Xu, B. The Central Role of Bicarbonate in the Electrochemical Reduction of Carbon Dioxide on Gold. *J. Am. Chem. Soc.* **2017**, *139*, 3774−3783.
(35) Niaura, G. Surface-enhanced Raman spectroscopic observation of two kinds of adsorbed OH^- ions at copper electrode. *Electrochim. Acta* **2000**, *45*, 3507−3519.
(36) Härtinger, S.; Pettinger, B.; Doblhofer, K. Cathodic formation of a hydroxyde adsorbate on copper (111) electrodes in alkaline electrolyte. *J. Electroanal. Chem.* **1995**, *397*, 335−338.
(37) Chan, H. Y. H.; Takoudis, C. G.; Weaver, M. J. Oxide film formation and oxygen adsorption on copper in aqueous media as probed by surface-enhanced Raman spectroscopy. *J. Phys. Chem. B* **1999**, *103*, 357−365.
(38) Zhao, Y.; Du, L.; Li, H.; Xie, W.; Chen, J. Is the Suzuki-Miyaura Cross-Coupling Reaction in the Presence of Pd Nanoparticles Heterogeneously or Homogeneously Catalyzed? An Interfacial Surface-Enhanced Raman Spectroscopy Study. *J. Phys. Chem. Lett.* **2019**, *10*, 1286−1291.
(39) Kim, S. M.; Hsu, A.; Lee, Y.-H.; Dresselhaus, M.; Palacios, T.; Kim, K. K.; Kong, J. The effect of copper pre-cleaning on graphene synthesis. *Nanotechnology* **2013**, *24*, 365602.
(40) Zhou, H.; Yu, W. J.; Liu, L.; Cheng, R.; Chen, Y.; Huang, X.; Liu, Y.; Wang, Y.; Huang, Y.; Duan, X. Chemical vapour deposition growth of large single crystals of monolayer and bilayer graphene. *Nat. Commun.* **2013**, *4*, 2096.
(41) Brown, G. M.; Hope, G. A. A SERS study of SO_4^{2-}/Cl^- ion adsorption at a copper electrode in-situ. *J. Electroanal. Chem.* **1996**, *405*, 211−216.
(42) Luc, W.; Ko, B. H.; Kattel, S.; Li, S.; Su, D.; Chen, J. G.; Jiao, F. SO_2-Induced Selectivity Change in CO_2 Electroreduction. *J. Am. Chem. Soc.* **2019**, *141*, 9902−9909.
(43) Jouny, M.; Lv, J.-J.; Cheng, T.; Ko, B. H.; Zhu, J.-J.; Goddard, W. A.; Jiao, F. Formation of carbon−nitrogen bonds in carbon monoxide electrolysis. *Nat. Chem.* **2019**, *11*, 846−851.
(44) Jouny, M.; Luc, W.; Jiao, F. High-rate electroreduction of carbon monoxide to multi-carbon products. *Nat. Catal.* **2018**, *1*, 748−755.
(45) Verdaguer-Casadevall, A.; Li, C. W.; Johansson, T. P.; Scott, S. B.; McKeown, J. T.; Kumar, M.; Stephens, I. E.; Kanan, M. W.; Chorkendorff, I. Probing the Active Surface Sites for CO Reduction on Oxide-Derived Copper Electrocatalysts. *J. Am. Chem. Soc.* **2015**, *137*, 9808−9811.
(46) Habekost, A. Experimental investigations of alkaline silver-zinc and copper-zinc batteries. *World J. Chem. Educ.* **2016**, *4*, 4−12.
(47) Sardari, B.; Özcan, M. Real-Time and Tunable Substrate for Surface-Enhanced Raman Spectroscopy by Synthesis of Copper Oxide Nanoparticles via Electrolysis. *Sci. Rep.* **2017**, *7*, 7730.
(48) Iijima, G.; Inomata, T.; Yamaguchi, H.; Ito, M.; Masuda, H. Role of a Hydroxide Layer on Cu Electrodes in Electrochemical CO_2 Reduction. *ACS Catal.* **2019**, *9*, 6305−6319.
(49) Li, F.; Thevenon, A.; Rosas-Hernández, A.; Wang, Z.; Li, Y.; Gabardo, C. M.; Ozden, A.; Dinh, C. T.; Li, J.; Wang, Y.; Edwards, J. P.; Xu, Y.; McCallum, C.; Tao, L.; Liang, Z.-Q.; Luo, M.; Wang, X.; Li, H.; O'Brien, C. P.; Tan, C.-S.; Nam, D.-H.; Quintero-Bermudez, R.; Zhuang, T.-T.; Li, Y. C.; Han, Z.; Britt, R. D.; Sinton, D.; Agapie, T.; Peters, J. C.; Sargent, E. H. Molecular tuning of CO_2-to-ethylene conversion. *Nature* **2020**, *577*, 509−513.
(50) Kim, Y.-G.; Javier, A.; Baricuatro, J. H.; Torelli, D.; Cummins, K. D.; Tsang, C. F.; Hemminger, J. C.; Soriaga, M. P. Surface reconstruction of pure-Cu single-crystal electrodes under CO-reduction potentials in alkaline solutions: A study by seriatim ECSTM-DEMS. *J. Electroanal. Chem.* **2016**, *780*, 290−295.
(51) Li, C. Y.; Dong, J. C.; Jin, X.; Chen, S.; Panneerselvam, R.; Rudnev, A. V.; Yang, Z. L.; Li, J. F.; Wandlowski, T.; Tian, Z. Q. In Situ Monitoring of Electrooxidation Processes at Gold Single Crystal Surfaces Using Shell-Isolated Nanoparticle-Enhanced Raman Spectroscopy. *J. Am. Chem. Soc.* **2015**, *137*, 7648−7651.
(52) Chernyshova, I. V.; Somasundaran, P.; Ponnurangam, S. On the origin of the elusive first intermediate of CO_2 electroreduction. *Proc. Natl. Acad. Sci. U. S. A.* **2018**, *115*, E9261−E9270.
(53) Chou, T.-C.; Chang, C.-C.; Yu, H.-L.; Yu, W.-Y.; Dong, C.-L.; Velasco-Vélez, J.-J.; Chuang, C.-H.; Chen, L.-C.; Lee, J.-F.; Chen, J.-M.; Wu, H.-L. Controlling the Oxidation State of Cu Electrode and Reaction Intermediates for Electrochemical CO_2 Reduction to Ethylene. *J. Am. Chem. Soc.* **2020**, *142*, 2857−2867.
(54) Li, C. W.; Ciston, J.; Kanan, M. W. Electroreduction of carbon monoxide to liquid fuel on oxide-derived nanocrystalline copper. *Nature* **2014**, *508*, 504−507.
(55) Handoko, A. D.; Chan, K. W.; Yeo, B. S. $-CH_3$ Mediated Pathway for the Electroreduction of CO_2 to Ethane and Ethanol on Thick Oxide-Derived Copper Catalysts at Low Overpotentials. *ACS Energy Lett.* **2017**, *2*, 2103−2109.
(56) Wang, L.; Nitopi, S. A.; Bertheussen, E.; Orazov, M.; Morales-Guio, C. G.; Liu, X.; Higgins, D. C.; Chan, K.; Nørskov, J. K.; Hahn, C.; Jaramillo, T. F. Electrochemical Carbon Monoxide Reduction on Polycrystalline Copper: Effects of Potential, Pressure, and pH on

https://dx.doi.org/10.1021/jacs.0c02354
J. Am. Chem. Soc. 2020, 142, 9735−9743

Selectivity toward Multicarbon and Oxygenated Products. *ACS Catal.* **2018**, *8*, 7445−7454.
(57) Tiwari, A.; Maagaard, T.; Chorkendorff, I.; Horch, S. Effect of Dissolved Glassware on the Structure-Sensitive Part of the Cu(111) Voltammogram in KOH. *ACS Energy Lett.* **2019**, *4*, 1645−1649.
(58) Leung, K. Y.; McCrory, C. C. L. Effect and Prevention of Trace Ag^+ Contamination from Ag/AgCl Reference Electrodes on CO_2 Reduction Product Distributions at Polycrystalline Copper Electrodes. *ACS Appl. Energy Mater.* **2019**, *2*, 8283−8293.

https://dx.doi.org/10.1021/jacs.0c02354
J. Am. Chem. Soc. 2020, 142, 9735−9743